metals

MDPI

Article

Separation of Manganese Oxides from Iron–Manganese Ores by Preliminary Hydrogen Reduction

Nurlybay Kosdauletov [1,2], Assylbek Nurumgaliyev [1,*], Galymzhan Adilov [1,2,*], Bakyt Suleimen [1,2], Bauyrzhan Kelamanov [2], Yerbol Kuatbay [1], Kagan Benzesik [3], Assylbek Abdirashit [1,2], Gulzat Bulekova [1] and Yeleussiz Nurassyl [2]

[1] Department of Metallurgy and Materials Science, Karaganda Industrial University, Temirtau 101400, Kazakhstan; n.kosdauletov@zhubanov.edu.kz (N.K.); b.suleimen@zhubanov.edu.kz (B.S.); ye.kuatbay@tttu.edu.kz (Y.K.); aabdirashit@zhubanov.edu.kz (A.A.)

[2] Department of Metallurgy and Mining, K. Zhubanov Aktobe Regional University, Aktobe 030000, Kazakhstan; bkelamanov@zhubanov.edu.kz (B.K.)

[3] Department of Metallurgical and Materials Engineering, Istanbul Technical University, Istanbaul 34469, Turkey; benzesik@itu.edu.tr

* Correspondence: a.nurumgaliyev@tttu.edu.kz (A.N.); g.adilov@zhubanov.edu.kz (G.A.); Tel.: +7-771-973-73-33 (G.A.)

Abstract

The present study investigates the possibility of selective iron reduction from the Keregetas iron–manganese ore deposit (Kazakhstan) using hydrogen, followed by the separation of iron- and manganese-containing phases. The relevance of the research is associated with the need to develop environmentally sustainable processing technologies for low-grade iron–manganese ores under the conditions of metallurgical industry decarbonization. Experimental studies were carried out at temperatures of 800–900 °C in a high-purity hydrogen atmosphere, followed by magnetic separation and liquid-phase separation of the reduction products. The phase and chemical compositions of the samples were analyzed using X-ray diffraction (XRD), scanning electron microscopy (SEM), and energy-dispersive spectroscopy (EDS). It was established that during the reduction process, iron oxides were predominantly transformed into the metallic state with the formation of α-Fe, whereas manganese oxides were mainly reduced to MnO and Mn_3O_4. Magnetic separation demonstrated limited selectivity due to the simultaneous transfer of iron-containing and manganese-containing phases into the magnetic fraction. At the same time, liquid-phase separation of the pre-reduced material at 1650 °C ensured effective separation of metallic and slag phases, with manganese concentrated in the slag and minimal losses in the metallic product. A technological flowsheet for the processing of iron–manganese ores is proposed, including hydrogen reduction, magnetic separation, and subsequent high-temperature phase separation. The obtained results demonstrate the prospects of hydrogen metallurgy for the development of low-carbon technologies for the integrated processing of iron–manganese raw materials.

Keywords: selective reduction; hydrogen; iron–manganese ores; manganese oxides; magnetic separation; component separation; hydrogen metallurgy; decarbonization

Check for updates

Academic Editor: Srecko Stopic

Received: 13 May 2026
Revised: 23 June 2026
Accepted: 23 June 2026
Published: 25 June 2026

Copyright: © 2026 by the authors. Licensee MDPI, Basel, Switzerland. This article is an open access article distributed under the terms and conditions of the Creative Commons Attribution (CC BY) license.

1. Introduction

Manganese is one of the key elements in modern metallurgy, playing a decisive role in the production of steels and cast irons due to its ability to bind harmful impurities and

act as an effective deoxidizing and alloying agent. The quality of manganese-containing raw materials directly affects the performance characteristics of metals, including their strength, wear resistance, and reliability. Ferromanganese production is traditionally based on the reduction of manganese ores using carbon or other reducing agents, enabling the production of a wide range of alloys with different compositions [1–4].

At the same time, the increasing demand for ferromanganese is accompanied by the growing problem of depletion of high-grade manganese ores. A significant portion of available raw materials is characterized by low manganese content and elevated levels of impurities (iron, silica, phosphorus), which negatively affect the efficiency of metallurgical processes, increase the consumption of reducing agents and energy, and complicate the control of the final product composition [5,6].

Under these conditions, the beneficiation of manganese ores becomes particularly important, aiming to improve their technological value and expand the raw material base of the metallurgical industry [7,8]. Various methods are used for processing ores of different genesis, including gravity concentration [9–11], magnetic separation [12,13], flotation [14–16], roasting followed by magnetic separation [17–20], hydrometallurgical processes [21–23], as well as pyrometallurgical methods of preliminary raw material treatment [24–27]. Despite the high efficiency of these approaches, they do not always provide the required raw material quality when processing low-grade and refractory ores.

The iron–manganese ores of Kazakhstan constitute an important part of the country's mineral resource base and are widely distributed, particularly within the Atasu basin, which includes the Zhezdy, Uspenskoye, and Karasai deposits [28]. These ores are characterized by a complex mineralogical composition (pyrolusite, manganite, braunite, psilomelane, hematite, magnetite) and often require preliminary treatment prior to metallurgical processing [29–31].

An additional factor influencing the development of manganese ore processing technologies is the global trend toward decarbonization of the metallurgical industry. Reducing CO_2 emissions and improving energy efficiency require reconsideration of both conventional smelting methods and the quality requirements for raw materials [32–36]. Under these conditions, increasing attention is being paid to technologies that provide more efficient reduction while minimizing the use of carbon-based reducing agents.

Particular interest in recent years has been focused on the use of hydrogen as a reducing agent, which is considered a promising approach for decreasing the carbon footprint of metallurgical processes [37–43]. However, the thermodynamic characteristics of the Mn–O–H system limit the possibility of complete reduction of manganese to the metallic state over a wide temperature range, as confirmed by Equations (1)–(4) [44–46]. In contrast to iron, manganese oxides exhibit a limited degree of reduction, creating favorable conditions for the selective reduction of iron-containing phases.

$$2MnO_2 + H_2\,(g) = Mn_2O_3 + H_2O\,(g)\ \Delta H\ (25\ ^\circ C) = -163.7\ kJ/mol \quad (1)$$

$$3Mn_2O_3 + H_2\,(g) = 2Mn_3O_4 + H_2O\,(g)\ \Delta H\ (25\ ^\circ C) = -135.1\ kJ/mol \quad (2)$$

$$Mn_3O_4 + H_2\,(g) = 3MnO + H_2O\,(g)\ \Delta H\ (25\ ^\circ C) = -16.6\ kJ/mol \quad (3)$$

$$MnO + H_2(g) \rightarrow Mn + H_2O(g),\ \Delta H\ (25\ ^\circ C) = +143\ kJ/mol \quad (4)$$

Previous studies have demonstrated the possibility of selective iron reduction while preserving manganese oxides, thereby opening prospects for the selective separation of components in iron–manganese ores [46–50]. Thermodynamic calculations made it possible to determine the temperature ranges at which maximum process selectivity can be achieved, as well as to identify the key factors influencing the equilibrium of reduction reactions [50].

Therefore, the aim of the present study is to investigate the possibilities of separating iron- and manganese-bearing phases after the preliminary selective reduction of iron–manganese ore with hydrogen, as well as to evaluate the effectiveness of magnetic separation and liquid-phase separation for obtaining separate iron-rich and manganese-rich products.

Thus, the development of technologies for the selective hydrogen reduction of iron from iron–manganese ores represents a relevant research direction that combines improved raw material processing efficiency with the potential to reduce the carbon footprint of metallurgical production.

In this regard, the aim of the present study is to investigate the processes of selective hydrogen reduction of iron from iron–manganese ores followed by its separation from manganese oxides, thereby improving the efficiency of raw material processing and advancing metallurgical technologies toward the requirements of a low-carbon economy.

2. Materials and Methods

Solid-state reduction of the iron–manganese ore was carried out in a vertical high-temperature furnace RB Automazione MM 6000 (MM 6000, RB Automazione, Genoa, Italy) equipped with electric heating and five independent temperature-control zones. The reaction system included a quartz tube with an inner diameter of approximately 75 mm, ensuring uniform heating of the sample. Experiments were performed at temperatures of 800 and 900 °C with an isothermal holding time of 60 min. Temperature was automatically controlled using a programmable controller and a thermocouple system, including a sensor positioned near the sample.

High-purity hydrogen (≥99.99% [51]) was used as the reducing gas at a flow rate of 0.5 L/min regulated by a digital mass flow controller. During heating and cooling, high-purity argon (≥99.993% [52]) was employed to maintain an inert atmosphere.

The separation smelting of samples preliminarily reduced at 900 °C was carried out in a resistance furnace (Nabertherm, Lilienthal, Germany) preheated to 1650 °C. The sample, placed in a corundum crucible, was held for 5 min, after which the melt was poured into a cast-iron mold followed by mechanical separation of the metallic and slag phases. After the reduction roasting, the samples consisted of a partially sintered material containing metallic and oxide phases. To liberate the phases and separate metallic iron particles from the oxide matrix prior to magnetic separation, the samples were additionally crushed to a particle size of less than 1 mm. The material was then processed using a Wet magnetic separator (CXG-ZN50 model, Jiangxi Victor International Mining Equipment Co., Ltd., Ganzhou, China) at a magnetic field intensity of 240 mT. The overall experimental procedure is presented in Figure 1.

For magnetic separation, the reduced samples were ground to a particle size below 1 mm and processed using a wet-type magnetic separator CXG-ZN50 at a magnetic field intensity of 240 mT (within the range of 230–320 mT). A mixture of distilled water and ethyl alcohol (4:1) with a total volume of 5 L per experiment was used as the working medium, while the sample mass was 20 g.

Microstructural analysis was performed after embedding the samples in epoxy resin with vacuum impregnation followed by polishing. Investigations were carried out in reflected light using an optical microscope and with a Scanning electron microscope equipped with an energy-dispersive X-ray spectroscopy (EDS) analyzer (JSM-7001F, JEOL Ltd., Akishima, Tokyo, Japan; X-Max 80, Oxford Instruments, Abingdon, UK) at an accelerating voltage up to 30 kV, with registration of secondary and backscattered electrons.

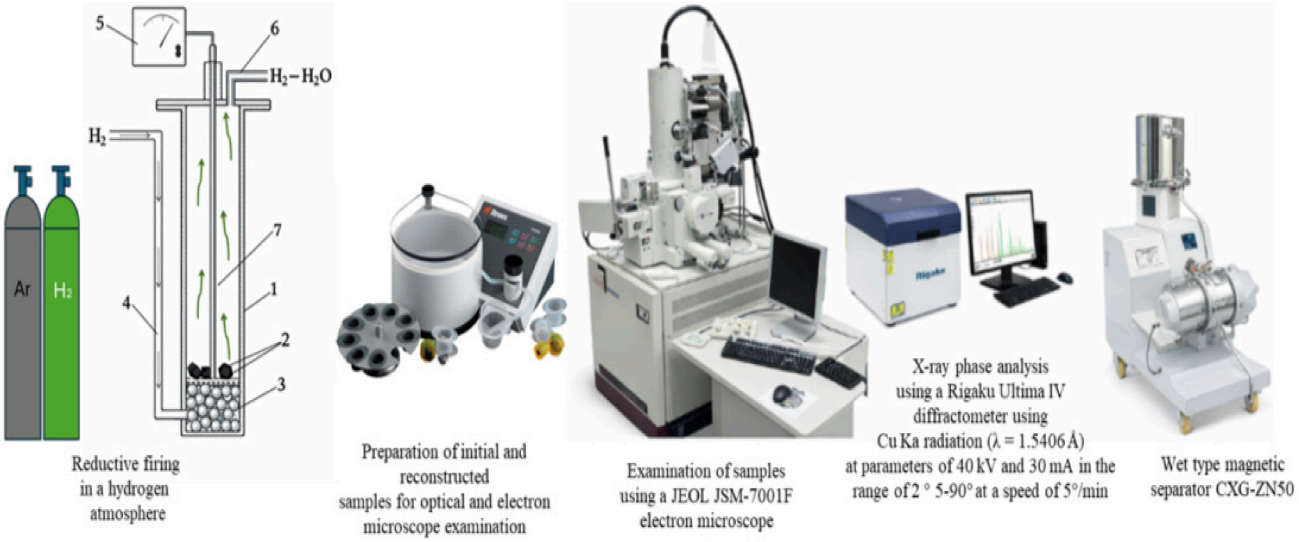


Figure 1. Schematic diagram of the experimental procedure.

The phase composition was determined by X-ray diffraction using a X-ray diffractometer (Ultima IV, Rigaku Corporation, Akishima, Tokyo, Japan) with Cu Kα radiation (λ = 1.5406 Å) operated at 40 kV and 30 mA in the 2θ range of 5–90° at a scanning rate of 5°/min. Powder samples with a particle size below 0.063 mm were prepared for analysis, and phase identification was performed using the Match! software package version 3.17 (Crystal Impact GbR, Bonn, Germany).

3. Results

3.1. Characterization of the Initial Iron–Manganese Ore

For the reduction experiments, the original iron–manganese ore was first ground in an IDA-175 mill to a particle size of −1 mm, which allowed significant homogenization of its chemical composition.

The ground ore sample was examined by scanning electron microscopy (SEM) in the backscattered electron imaging mode (Figure 2, Table 1).

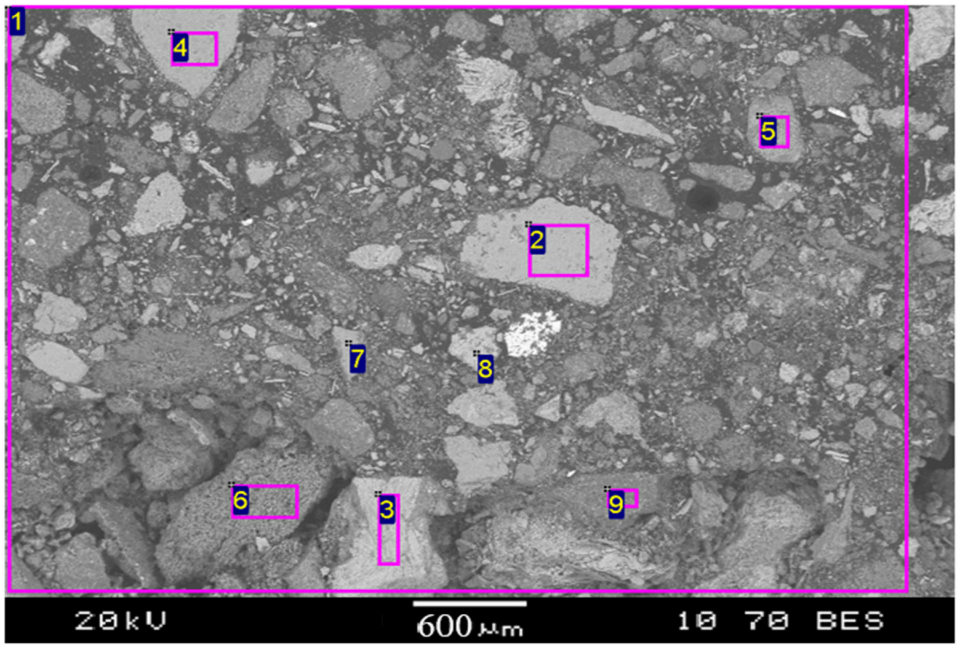


Figure 2. Ground iron–manganese ore.

Table 1. Chemical composition of the iron–manganese ore after grinding.

Spectrum	O	Al	Si	K	Ca	Mn	Fe	As	Ba
1	68.5	3.6	11.5	1.8	0.4	8.2	5.6	ND	0.3
2	69.1	0.4	0.7	2.9	ND	26.8	ND	ND	ND
3	69.9	ND	1.1	ND	0.6	0.9	27.6	0.4	ND
4	71.6	1.8	1.0	1.4	0.3	22.9	1.0	ND	ND
5	70.7	ND	10.9	0.3	0.3	17.0	0.7	ND	0.1
6	72.3	5.5	16.1	4.2	ND	0.5	1.1	ND	0.3
7	71.7	0.8	2.1	0.7	0.6	20.4	3.7	ND	ND
8	57.3	0.5	1.8	ND	ND	13.6	26.8	ND	ND
9	71.7	5.9	17.0	0.2	1.2	2.3	1.2	ND	0.6

Note: ND—not detected (below the limit of quantification, LOQ).

The microanalysis data clearly distinguish the main phase constituents of the Keregetas iron–manganese ore. Manganese-rich phases are distinctly localized in the regions corresponding to spectra 2, 4, 5, and 7. The highest manganese concentration was recorded in spectrum 2, reaching 26.8 at.% with virtually no iron present. In spectra 4, 5, and 7, the manganese content ranges from 17.0 to 22.9 at.% with only minor iron concentrations (not exceeding 3.7 at.%), indicating the predominance of independent manganese oxide or hydroxide mineral phases that are effectively liberated during grinding.

In addition to manganese-rich phases, distinct iron-rich and mixed iron–manganese inclusions were identified in the ground sample. Spectrum 3 represents an iron-rich phase containing 27.6 at.% Fe and only 0.9 at.% Mn, together with a minor arsenic impurity of 0.7 at.%. The mixed nature of the Keregetas ore is clearly illustrated by spectrum 8, which exhibits simultaneously high concentrations of both target elements, namely 26.8 at.% Fe and 13.6 at.% Mn.

The host rock is predominantly represented by an aluminosilicate matrix, most clearly observed in spectra 6 and 9. These regions are characterized by high concentrations of silicon (16.1–17.0 at.%) and aluminum (5.5–5.9 at.%), together with elevated potassium contents reaching 4.2 at.% in spectrum 6. The total concentration of ore-forming elements within the silicate regions does not exceed 3.5 at.%, confirming their association with gangue minerals. Spectrum 1, which covers a large area of the investigated section, represents the average composition of the ground ore fraction (−1 mm), combining characteristics of both the silicate matrix (11.5 at.% Si) and manganese and iron oxides (8.2 at.% Mn and 5.3 at.% Fe).

A detailed mineralogical, phase, and chemical characterization of the Keregetas iron–manganese ore was previously presented in Ref. [48]. According to the results of X-ray diffraction and electron microprobe analyses, the ore is characterized by a complex and heterogeneous composition consisting of iron and manganese oxides as well as mixed Fe–Mn oxide phases. The presence of minerals based on Fe_2O_3, MnO_2, and mixed oxides of the Fe–Mn–O system was established, indicating a close mineralogical association between iron and manganese within the ore structure. These characteristics of the raw material have a significant influence on the processes of selective reduction and the subsequent separation of iron- and manganese-bearing components.

The obtained material shown in Figure 2 was mixed with water to impart shape to the samples. After shaping, the samples were dried in a drying oven at 150 °C for 1 h in order to remove residual moisture. Reduction experiments were carried out at temperatures of 800 and 900 °C with an isothermal holding time of 60 min. The selection of the reduction roasting temperature was based on the results of previously conducted thermodynamic

calculations and experimental studies. The selection of reduction roasting temperatures in the range of 800–900 °C was based on the results of previously conducted thermodynamic calculations and experimental studies on the selective hydrogen reduction of the Keregetas iron–manganese ore [48,50].

3.2. Results of Hydrogen Reduction and Magnetic Separation

Figure 3 presents the X-ray diffraction analysis of the samples after magnetic separation performed following reduction roasting at temperatures of 800–900 °C. The analysis was carried out using a Rigaku Ultima IV diffractometer, while the diffraction patterns were interpreted using the Match! software package (Crystal Impact, Germany).

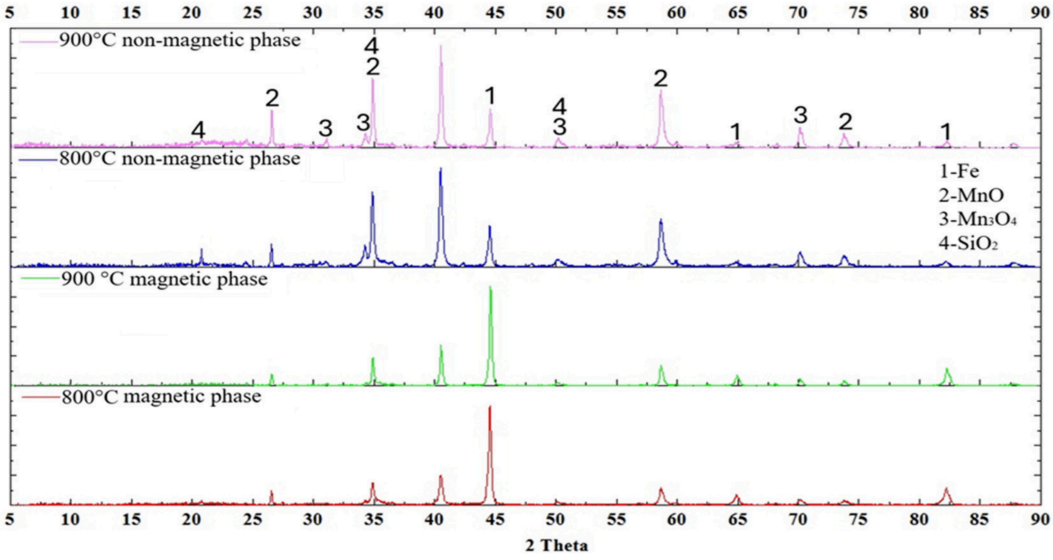


Figure 3. X-ray diffraction analysis of samples after magnetic separation at temperatures of 800–900 °C.

According to the analysis results, the magnetic fraction exhibited a significant increase in the intensity of peaks corresponding to iron compared with previously published data [50], indicating an increased concentration of iron-containing minerals in this fraction. In contrast, the non-magnetic fraction showed high-intensity peaks corresponding to manganese and silicon oxides, indicating their predominant accumulation in the non-magnetic portion of the material.

Quantitative phase analysis performed using the Rietveld method showed that at 900 °C the magnetic fraction is dominated by α-Fe (39.9%) and MnO (38.8%) phases. In addition, the sample contains quartz SiO_2 in an amount of 14.1% and manganese oxide Mn_3O_4 at 7.3%.

Figure 4 presents the appearance of the samples reduced by hydrogen at 900 °C and subsequently subjected to magnetic separation using a CXG-ZN50 wet-type magnetic separator. As a result of the separation process, the magnetic fraction accounted for 33% of the total sample mass, while the remaining portion was transferred into the non-magnetic fraction.

Spectral analysis of the separated products showed that iron-containing components predominantly passed into the magnetic fraction. This fraction also contains manganese oxides, which can be effectively separated during subsequent processing stages, for example, by smelting (Figure 4, Table 2).

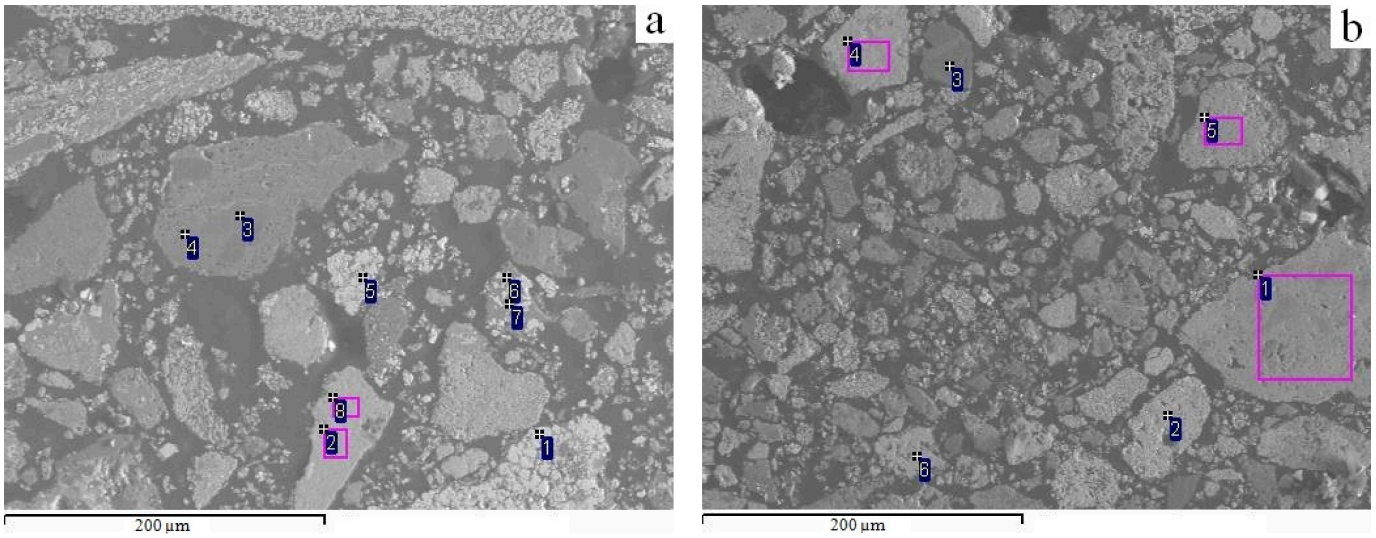


Figure 4. Appearance of hydrogen-reduced samples at 900 °C after magnetic separation: magnetic (**a**) and non-magnetic fractions (**b**).

Table 2. Chemical composition of samples after magnetic separation: magnetic fraction (a) and non-magnetic fraction (b).

Spectrum	O	Al	Si	K	Ca	Mn	Fe	Ba
1 (a)	ND	ND	ND	ND	ND	1.13	98.87	ND
2 (a)	46.30	0.86	3.24	0.33	0.49	45.07	3.22	0.49
3 (a)	54.05	9.04	28.62	7.95	ND	ND	0.34	ND
4 (a)	56.94	8.75	26.69	6.65	0.00	ND	0.65	0.31
5 (a)	ND	ND	ND	ND	ND	2.40	97.60	ND
6 (a)	ND	ND	ND	ND	ND	1.18	98.82	ND
7 (a)	54.63	0.62	29.74	9.23	ND	1.47	4.31	ND
8 (a)	48.51	1.63	3.49	0.83	0.55	38.86	5.86	0.26
1 (b)	51.03	1.17	26.55	0.34	0.47	19.22	1.21	ND
2 (b)	46.48	ND	8.21	ND	ND	39.41	5.89	ND
3 (b)	57.11	ND	42.45	ND	ND	0.44	ND	ND
4 (b)	43.92	ND	ND	ND	0.27	53.49	2.31	ND
5 (b)	50.96	0.95	22.77	0.31	0.30	23.79	0.94	ND

Note: ND—not detected (below the limit of quantification, LOQ).

The non-magnetic fraction is represented by oxide components of the iron–manganese ore that were not reduced under the given conditions. Its composition mainly consists of manganese, silicon, aluminum, and calcium oxides, as well as manganese and silicon silicates partially dissolved in the crystal lattice of minerals.

Thus, the obtained results indicate that magnetic separation does not provide complete selective separation of iron- and manganese-bearing phases. However, it enables the concentration of a significant portion of the reduced iron in the magnetic product for subsequent processing, since both iron-containing and manganese-containing phases are transferred to the magnetic fraction. The substantial presence of MnO together with α-Fe indicates the lack of selectivity of the magnetic separation process under the investigated conditions.

3.3. Liquid-Phase Separation of the Reduced Ore

Figure 5 presents the sample reduced at 900 °C (a), its X-ray diffraction pattern (b), and the appearance of the metal (c) and slag (d) after smelting, as well as the chemical composition of the elements present in the metal and slag after separation smelting of the iron–manganese ore (Table 3).

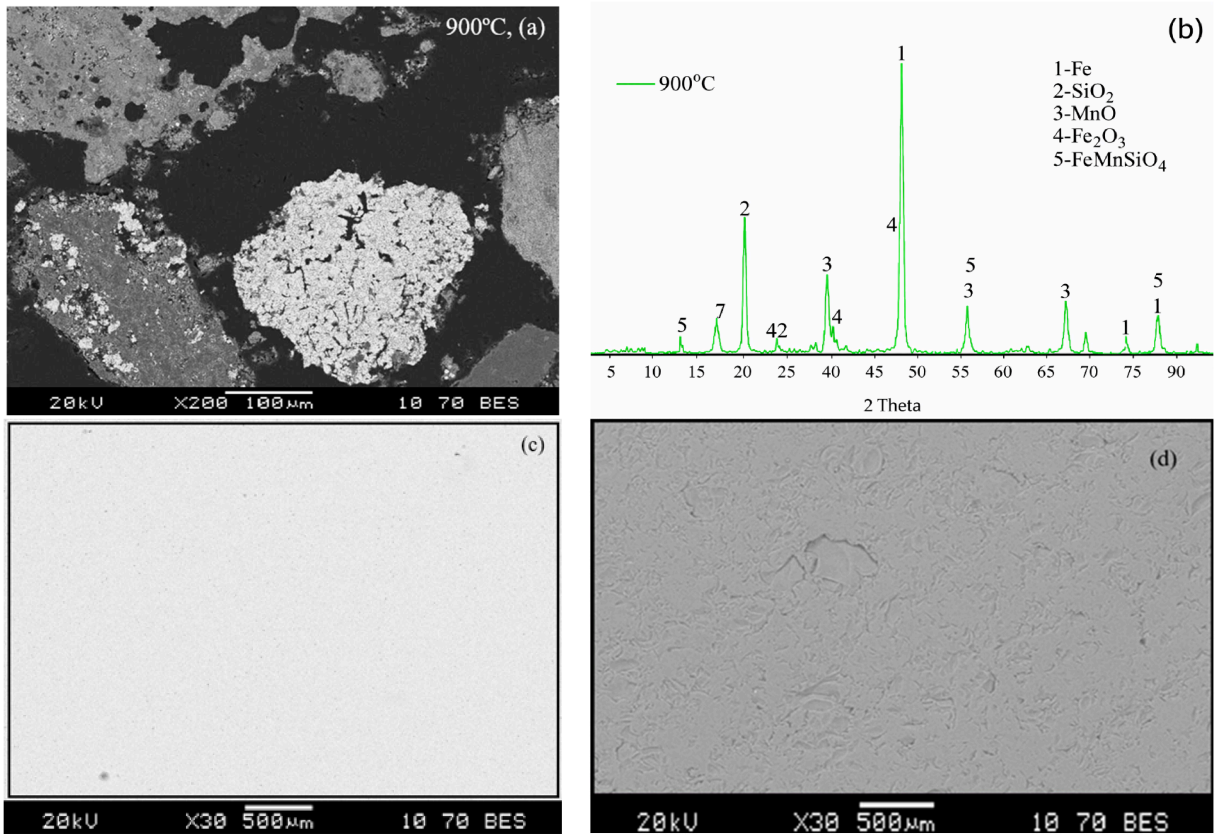


Figure 5. Sample reduced at 900 °C (**a**) SEM image; (**b**) X-ray diffraction pattern (XRD); (**c**) appearance of the obtained metal; (**d**) appearance of the slag after melting, indicating the analysis area.

Table 3. Compositions of the metal and slag after separation smelting, wt.%.

Product	Analysis Area	O	Al	Si	K	Ca	Mn	Fe	As
Metal	Spectrum 1 (c)	ND	ND	ND	ND	ND	ND	93.66	6.34
Slag	Spectrum 1 (d)	32.65	9.40	17.92	1.65	1.03	29.38	7.98	ND

Note: ND—not detected (below the limit of quantification, LOQ).

The micrograph obtained using a scanning electron microscope at a magnification corresponding to 100 µm clearly shows the presence of two main phases in the sample—metallic and oxide phases. The results of the X-ray diffraction analysis confirm this observation.

In Figure 5c,d, the uniform bright background of the metallic phase and the homogeneous gray background of the slag indicate a high degree of chemical homogeneity. This suggests a uniform distribution of atoms of the various elements identified in the characteristic radiation spectra, both in the quenched metal and in the quenched slag. The chemical compositions of the metal and slag are presented in Table 3.

Thus, liquid-phase separation of the hydrogen-pre-reduced iron–manganese ore demonstrates high efficiency, since manganese was not detected in the separated metallic

phase and its losses in the form of accompanying metal are eliminated. This significantly distinguishes the method from magnetic separation.

Based on the obtained results, a processing flowsheet for iron–manganese ore can be proposed, including preliminary reduction, magnetic separation, and subsequent liquid-phase separation of the magnetic fraction in order to separate the residual manganese oxide, thereby eliminating manganese losses. As a result of this process, it becomes possible to obtain a metallic product and an oxide concentrate enriched in manganese. The proposed general processing flowsheet for iron–manganese ores is presented in Figure 6.

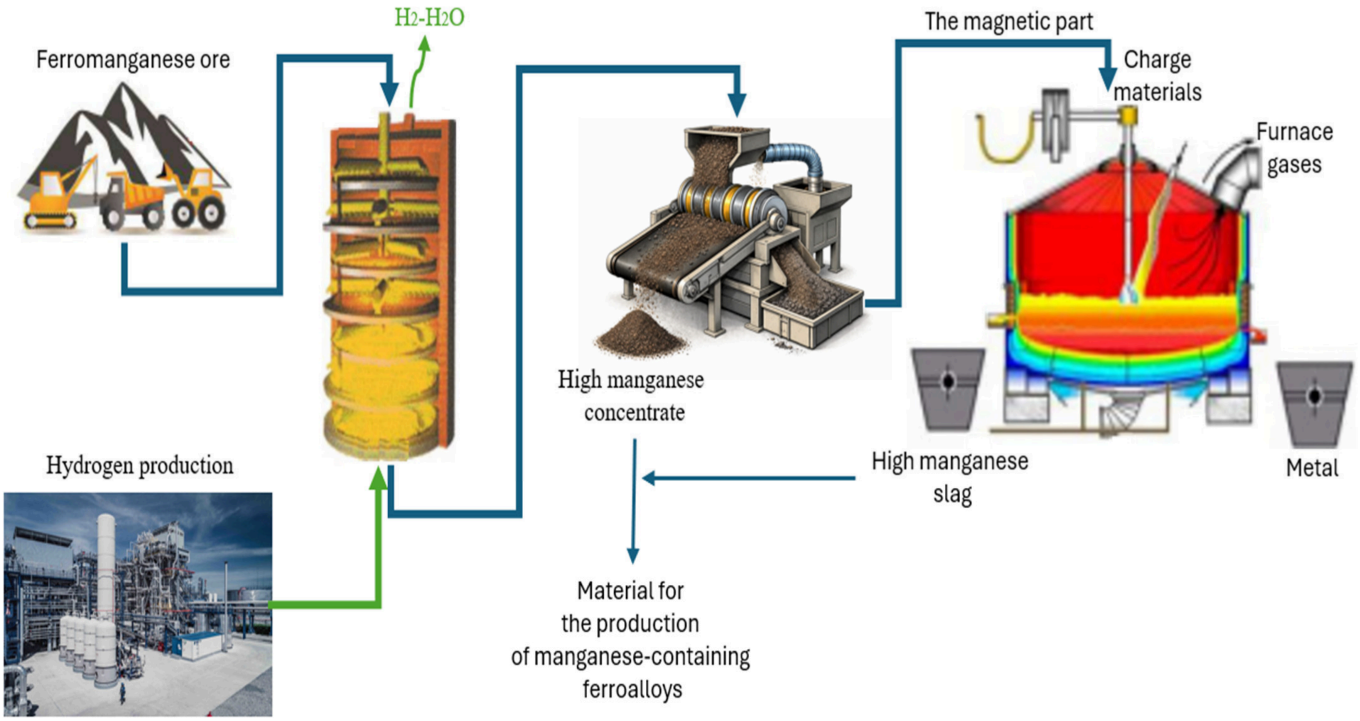


Figure 6. Proposed flowsheet for producing a high-manganese material from iron–manganese ores.

4. Discussion

Investigation of the initial iron–manganese ore over the sample surface area showed that the ore is heterogeneous and contains various mineral phases. The main elements are Fe, Mn, and Si; in addition, complex phases such as Fe_2MnO_4 are present, indicating a close mineralogical association between iron and manganese within the ore structure (Figure 2). During reduction roasting in a hydrogen atmosphere at 800–900 °C, the reduction of iron oxides proceeds first according to the reaction:

$$Fe_2O_3 + 3H_2 \rightarrow 2Fe + 3H_2O; \quad (5)$$

$$Fe_3O_4 + 4H_2 \rightarrow 3Fe + 4H_2O, \quad (6)$$

which leads to the formation of metallic iron, whereas manganese oxides are reduced to a much lesser extent and predominantly transform into monoxide according to the reaction:

$$MnO_2 + H_2 \rightarrow MnO + H_2O \quad (7)$$

The presence of mixed oxide phases such as Fe_2MnO_4 promotes the simultaneous occurrence of reduction processes and redistribution of components within the solid phase. Magnetic separation performed using a CXG-ZN50 wet-type magnetic separator showed that 33% of the total sample mass was transferred into the magnetic fraction. According to

the X-ray diffraction analysis results, the magnetic fraction exhibited an increased intensity of peaks corresponding to α-Fe, while the presence of MnO and Mn_3O_4 oxides was also detected (Figure 3).

Liquid-phase separation of the hydrogen-pre-reduced sample at 900 °C demonstrated that the obtained concentrate can be effectively separated into metallic and slag phases without manganese losses into the metallic product. According to the data presented in Table 3, after separation arsenic is present in the metal in the form of a solid solution in iron in an amount of 6.34 wt.% (Figure 5, Spectrum 1c).

Thus, liquid-phase separation of the iron–manganese ore pre-reduced with hydrogen demonstrates high efficiency, since manganese was not detected in the separated metallic phase and its losses as an accompanying metal are completely eliminated. This distinctly differentiates the method from magnetic separation.

In contrast to conventional carbothermic reduction of iron–manganese ores, the use of hydrogen enables the selective reduction of iron at temperatures of 800–900 °C without significant reduction of manganese to the metallic state. This creates favorable conditions for the subsequent separation of iron- and manganese-bearing phases. Furthermore, when low-carbon ("green") hydrogen is employed, the process has the potential to significantly reduce CO_2 emissions compared with technologies based on carbon-containing reducing agents.

5. Conclusions

In this study, the phase composition and processing behavior of iron–manganese ore were investigated under hydrogen reduction and subsequent separation routes. The main conclusions can be summarized as follows:

1. The studied ore exhibits a complex and heterogeneous phase composition, where iron and manganese are closely associated, including the formation of mixed oxide phases such as Fe_2MnO_4. This mineralogical intergrowth significantly limits selective separation.

2. Hydrogen reduction at 800–900 °C leads to the preferential reduction of iron to metallic α-Fe. However, subsequent magnetic separation is not selective, as manganese oxides (MnO and Mn_3O_4) are co-recovered in the magnetic fraction.

3. Liquid-phase separation at 1650 °C of the pre-reduced material ensures efficient phase segregation into metallic and slag phases. Manganese is predominantly concentrated in the slag (up to ~45% MnO), with negligible losses to the metallic product.

4. The combination of hydrogen-based reduction and liquid-phase separation is demonstrated to be an effective processing route for iron–manganese ores, enabling high selectivity and minimizing losses of valuable components such as Mn and Si.

5. The proposed flowsheet, including hydrogen reduction, magnetic separation, and subsequent high-temperature liquid-phase treatment, provides a promising basis for the development of industrially scalable and low-carbon technologies, particularly when hydrogen produced from renewable energy sources is used as the reducing agent.

Overall, the results contribute to the advancement of sustainable processing strategies for complex iron–manganese raw materials and highlight the potential of hydrogen metallurgy in future metallurgical applications.

Author Contributions: Conceptualization, A.N. and G.A.; methodology, N.K., A.N., B.S. and K.B.; software, Y.K. and Y.N.; validation, G.A., B.K., K.B. and A.A.; formal analysis, N.K., A.A., A.N. and K.B.; investigation, N.K., B.S., A.A. and G.B.; resources, G.A., B.K. and Y.N.; data curation, G.B., Y.N. and Y.K.; writing—original draft preparation, N.K., Y.K., B.S. and A.N.; writing—review and editing, G.A., B.K., K.B., A.A. and Y.N.; visualization, Y.K., Y.N., G.B. and K.B.; supervision, G.A., B.K. and A.N.; project administration, A.N. and G.A.; funding acquisition, A.N. and G.A. All authors have read and agreed to the published version of the manuscript.

Funding: This research is funded by the Science Committee of the Ministry of Science and Higher Education of the Republic of Kazakhstan (Grant No. AP 23490490).

Data Availability Statement: The original contributions presented in this study are included in the article. Further inquiries can be directed to the corresponding authors.

Acknowledgments: The authors express their sincere gratitude to K. Zhubanov Aktobe Regional University, Karaganda Industrial University, and South Ural State University (Research Laboratory "Hydrogen Technologies in Metallurgy") for their administrative and technical support, as well as for providing the facilities and resources necessary to conduct this research.

Conflicts of Interest: The authors declare no conflict of interest.

References

1. Dashevskii, V.Y.; Aleksandrov, A.A.; Zhuchkov, V.I.; Leontev, L.I. The manganese problem in Russian metallurgy. *Izv. Ferr. Metall.* **2020**, *63*, 579–590. [CrossRef]
2. Dashevskii, V.Y.; Yusfin, Y.S.; Aleksandrov, A.A.; Leontev, L.I.; Podgorodetskii, G.S.; Gubanov, V.I. Increasing the efficient utilization of manganese in the production of manganese ferroalloys. *Izv. Ferr. Metall.* **2013**, *56*, 32–37.
3. Dashevskii, V.Y.; Yusfin, Y.S.; Podgorodetskii, G.S.; Baeva, N.V. Production of manganese ferroalloys from manganese ores of the Usinsk deposit. *Izv. Ferr. Metall.* **2013**, *56*, 9–16.
4. Dashevskii, V.Y.; Aleksandrov, A.A.; Leontev, L.I. Thermodynamics of oxygen solutions in Ni-Co melts containing manganese. *Izv. Ferr. Metall.* **2019**, *62*, 475–483. [CrossRef]
5. Singh, V.; Chakraborty, T.; Tripathy, S.K. A review of low-grade manganese ore upgradation processes. *Miner. Process. Extr. Metall. Rev.* **2020**, *41*, 417–438. [CrossRef]
6. Clarke, C.; Upton, S. A global portrait of the manganese industry-A socioeconomic perspective. *Neurotoxicology* **2017**, *58*, 173–179. [CrossRef] [PubMed]
7. Cheraghi, A.; Yoozbashizadeh, H.; Safarian, J. Gaseous reduction of manganese ores: A review and theoretical insight. *Miner. Process. Extr. Metall. Rev.* **2020**, *41*, 198–215.
8. Kelamanov, B.; Tolymbekov, M.; Kaskin, K.; Baisanov, A. Thermal analysis of agglomerated nickel ore. In Proceedings of the 12th International Ferroalloys Congress: Sustainable Future, Helsinki, Finland, 6–9 June 2010; pp. 657–659.
9. Souza, H.S.; Braga, A.S.; Oliveira, A.H. Concentration of manganese tailings via reverse flotation in an acid medium. *REM Int. Eng. J.* **2016**, *69*, 85–90. [CrossRef]
10. Mishra, P.P.; Mohapatra, B.K.; Mahanta, K. Upgradation of low-grade siliceous manganese ore from Bonai-Keonjhar Belt, Orissa, India. *J. Miner. Mater. Charact. Eng.* **2009**, *8*, 47–56. [CrossRef]
11. Malayoğlu, U. Study on the gravity processing of manganese ores. *Asian J. Chem.* **2010**, *22*, 2379–2386.
12. Mishra, S.; Mohapatra, B.K.; Dash, N.; Rao, D.S. Ore petrography of low-grade siliceous manganese ores from the Bonai-Keonjhar belt, Orissa, India: Influence of mineral fabric on beneficiation. *Min. Sci. Technol.* **2011**, *21*, 803–808. [CrossRef]
13. Grieco, G.; Kastrati, S.; Pedrotti, M. Magnetic enrichment of braunite-rich manganese ore at different grain sizes. *Miner. Process. Extr. Metall. Rev.* **2014**, *35*, 257–265. [CrossRef]
14. Mokrini, F.; Waeyenberge, L.; Viaene, N.; Moens, M. First report of the cereal cyst nematode Heterodera latipons on wheat in Morocco. *Plant Dis.* **2012**, *96*, 774. [CrossRef] [PubMed]
15. Luo, N.; Wei, D.Z.; Shen, Y.B.; Liu, W.G.; Gao, S.L. Effect of calcium ion on the separation of rhodochrosite and calcite. *J. Mater. Res. Technol.* **2018**, *7*, 96–101. [CrossRef]
16. Calderon-Rodarte, J.; Lopez-Valdivieso, A.; Aragon-Pina, A.; Reyes-Bahena, J.L.; Gallegos-Garcia, M.I.; Zapata-Velazquez, A.; Robledo-Cabrera, A. Mineralogy and silver distribution in argentiferous manganese ores from La Encantada mines in Mexico. *Physicochem. Probl. Miner. Process.* **2017**, *53*, 591–600. [CrossRef]
17. Gao, Y. *Prereduction and Magnetic Separation of Low Grade Manganese Ore*; The University of Utah: Salt Lake City, UT, USA, 2011.
18. Gao, Y.; Olivas-Martinez, M.; Sohn, H.Y.; Kim, H.G.; Kim, C.W. Upgrading of low-grade manganese ore by selective reduction of iron oxide and magnetic separation. *Metall. Mater. Trans. B* **2012**, *43*, 1465–1475. [CrossRef]
19. Mpho, M.; Samson, B.; Ayo, A. Evaluation of reduction roasting and magnetic separation for upgrading Mn/Fe ratio of fine ferromanganese ore. *Int. J. Min. Sci. Technol.* **2013**, *23*, 537–541. [CrossRef]
20. Pereira, M.J.; Lima, M.M.; Lima, R.M. Calcination and characterization studies of a Brazilian manganese ore tailing. *Int. J. Miner. Process.* **2014**, *131*, 26–30. [CrossRef]
21. You, Z.; Li, G.; Peng, Z.; Qin, L.; Zhang, Y.; Jiang, T. Reductive roasting of iron-rich manganese oxide ore with elemental sulfur for selective manganese extraction. *J. Min. Metall. B Metall.* **2017**, *53*, 115–122. [CrossRef]

22. Zhang, W.; Singh, P.; Muir, D.D. Oxidative precipitation of manganese with SO_2/O_2 and separation from cobalt and nickel. *Hydrometallurgy* **2002**, *63*, 127–135. [CrossRef]
23. Zhang, W.S.; Cheng, C.Y. Manganese metallurgy review. Part II: Manganese separation and recovery from solution. *Hydrometallurgy* **2007**, *89*, 160–177. [CrossRef]
24. Olsen, S.E.; Tangstad, M.; Lindstad, T. *Production of Manganese Ferroalloys*; Tapir Academic Press: Trondheim, Norway, 2007.
25. Tathavadkar, V.; Singh, V.; Mishra, P.K.; Mallick, P.; Nanda, B.D. Effect of manganese ore blends on performance of submerged arc furnace for ferromanganese production. *Ironmak. Steelmak.* **2010**, *37*, 103–111. [CrossRef]
26. Peng, E.; Yang, J.; Wang, Z.; Li, D.; Gao, Y.; Yan, D.; Chen, Y.; Guo, X. Manganese Resources in China: An Overview of Resource Status and Recent Advances in Metallogenic Models and Exploration. *Minerals* **2025**, *15*, 859. [CrossRef]
27. Li, Y.; Pan, X.; Amini Horri, B. Advancements in Sustainable Electrolytic Manganese Recovery: Techniques, Mechanisms, and Future Trends. *Recycling* **2025**, *10*, 26. [CrossRef]
28. Baisanov, A.; Maishina, Z.; Isagulov, A.; Smagulova, N.; Yudakova, V. Experimental melting of high-silicon ferromanganese with the use of ferromanganese ore and manganese slag. *Metalurgija* **2021**, *60*, 89–92.
29. Raimbekova, A.; Kubekova, S.; Kapralova, V.; Rysbekov, K.; Dalbanbay, A.; Ibraimova, G.; Mukhanov, A. Zhayrem overburden acid leaching study. *Chem. J. Kaz.* **2025**, *2*, 25–32. [CrossRef]
30. Toleukadyr, R.T.; Gabdullin, S.T.; Shabanov, E.Z.; Baisanov, A.S.; Salimgerei, N.A. Thermodynamic modeling of ferrosilicomanganese smelting using the TERRA software package. *Nauka Tekhnika Kazakhstana* **2021**, *4*, 87–95.
31. Kosdauletov, N.; Suleimen, B.; Adilov, G.; Senin, A.V.; Roshchin, V.E. Production of specification-grade ferrosilicomanganese from off-grade Fe–Mn ores. *Russ. Metall.* **2025**, *2025*, 1495–1500. [CrossRef]
32. Leshchinskaya, A.F.; Skorokhod, A.M. Influence of financial instruments, ESG principles, and carbon regulation on the metallurgical industry. *Russ. J. Ind. Econ.* **2022**, *15*, 297–307. [CrossRef]
33. Du, Z.; Lin, B. Analysis of carbon emissions reduction in China's metallurgical industry. *J. Clean. Prod.* **2018**, *176*, 1177–1184. [CrossRef]
34. Hu, R.; Zhang, Q. Study of a low-carbon production strategy in the metallurgical industry in China. *Energy* **2015**, *90*, 1456–1467. [CrossRef]
35. Adilov, G.; Suleimen, B.; Kosdauletov, N. Challenges and opportunities in the recycling of copper slags. *J. Sustain. Metall.* **2025**, *11*, 2064–2074. [CrossRef]
36. Zhang, J.; Shen, J.; Xu, L.; Zhang, Q. The CO2 emission reduction path toward carbon neutrality in the Chinese steel industry: A review. *Environ. Impact Assess. Rev.* **2023**, *99*, 107017. [CrossRef]
37. Roshchin, V.E.; Roshchin, A.V. Electrochemistry of reduction processes and prospects for the development of reduction technologies. *Izv. Ferr. Metall.* **2025**, *68*, 424–433. [CrossRef]
38. Kelamanov, B.; Yessengaliyev, D.; Sariev, O.; Akuov, A.; Samuratov, Y.; Zhuniskaliyev, T.; Kuatbay, Y.; Mukhambetgaliyev, Y.; Kolesnikova, O.; Zhumatova, A.; et al. Technological Analysis of the Production of Nickel-Containing Composite Materials. *J. Compos. Sci.* **2024**, *8*, 179. [CrossRef]
39. Smirnov, K.I.; Gamov, P.A.; Roshchin, V.E.; Samolin, V.S. Thermodynamic analysis of conditions for iron and titanium separation in ilmenite concentrate by selective reduction of elements. *Izv. Ferr. Metall.* **2025**, *68*, 171–178. [CrossRef]
40. Smirnov, K.I.; Gamov, P.A.; Samolin, V.S.; Roshchin, V.E. Selective reduction of iron from ilmenite concentrate. *Chern. Met.* **2024**, *7*, 19–23. [CrossRef]
41. Roshchin, V.E.; Drozin, A.D.; Gamov, P.A.; Smirnov, K.I. Decarbonization of steelmaking from the standpoint of the electronic theory of metal reduction. *Russ. Metall.* **2024**, *2024*, 529–536. [CrossRef]
42. Tian, P.; Gao, P.; Wang, M.; Li, Y.; Han, Y. Pilot-scale recovery of iron from refractory specularite ore using hydrogen-based mineral phase transformation technology: Process optimization, mineral characterization, and green production. *J. Clean. Prod.* **2025**, *491*, 144836. [CrossRef]
43. Ning, J.; Gao, P.; Wang, Y.; Yuan, S.; Sun, Y.; Li, W.; Tang, Z. Mineralogical characterization and flotation properties of rare earths in refractory iron tailings subjected to hydrogen-based mineral phase transformation. *Int. J. Miner. Metall. Mater.* **2025**, *32*, 1309–1321. [CrossRef]
44. He, J.; Guo, L.; Gao, P.; Zhu, X.; Yuan, S.; Wang, Z.; Han, Y. Recovery of strategic mineral resources such as iron and rare earth from long-stockpiled solid waste: Low-temperature fluidized reduction process and hydrogen substitution for carbon. *Sep. Purif. Technol.* **2025**, *360*, 131233. [CrossRef]
45. Safarian, J. A Sustainable Process to Produce Manganese and Its Alloys through Hydrogen and Aluminothermic Reduction. *Processes* **2022**, *10*, 27. [CrossRef]
46. Kumar, P.; Safarian, J. Sustainable production of ultra-low-carbon ferromanganese and calcium aluminate slag from pre-reduced manganese ore using aluminium. *Can. Metall. Q.* **2025**, 1–22. [CrossRef]
47. Suleimen, B.; Kosdauletov, N.; Adilov, G. Dephosphorization of high-phosphorus oolitic iron ore by prereduction with carbon monoxide followed by smelting. *Open Chem. Eng. J.* **2025**, *19*, e18741231409126. [CrossRef]

48. Kosdauletov, N.; Nurumgaliyev, A.; Zhautikov, B.; Suleimen, B.; Adilov, G.; Kelamanov, B.; Smirnov, K.; Zhuniskaliyev, T.; Kuatbay, Y.; Bulekova, G.; et al. Selective reduction of iron from iron–manganese ore of the Keregetas deposit using hydrogen. *Metals* **2025**, *15*, 691. [CrossRef]
49. Abdirashit, A.; Suleimen, B.; Uakhitova, B.; Uakhitov, R.; Taizhigitova, M.; Nurtayev, A. Thermodynamic and Pilot-Scale Experimental Analysis of Medium-Carbon Ferromanganese Production. *Metals* **2026**, *16*, 240. [CrossRef]
50. Kosdauletov, N.; Suleimen, B.; Adilov, G. The effect of various reducing agents on the process of solid-phase reduction of highly phosphorus ferromanganese ore. *Open Chem. Eng. J.* **2025**, *19*, e18741231398815. [CrossRef]
51. *GOST 3022-80*; Metals. Methods for Determination of Density. Izdatelstvo Standartov: Moscow, Russia, 1980.
52. *GOST 10157-2016*; Fireclay Refractories. Specifications. Standartinform: Moscow, Russia, 2016.

Disclaimer/Publisher's Note: The statements, opinions and data contained in all publications are solely those of the individual author(s) and contributor(s) and not of MDPI and/or the editor(s). MDPI and/or the editor(s) disclaim responsibility for any injury to people or property resulting from any ideas, methods, instructions or products referred to in the content.